SCIENCE CHINA
Physics, Mechanics & Astronomy

• Article •

February 2023 Vol. 66 No. 2: 227511
https://doi.org/10.1007/s11433-022-1973-x

Intrinsic anomalous spin Hall effect

Ping Li[1,2], Jing-Zhao Zhang[1], Zhi-Xin Guo[1,2*], Tai Min[1], and Xiangrong Wang[3,4*]

[1] *State Key Laboratory for Mechanical Behavior of Materials, Center for Spintronics and Quantum System, School of Materials Science and Engineering, Xi'an Jiaotong University, Xi'an 710049, China;*
[2] *Key Laboratory for Computational Physical Sciences (Ministry of Education), Fudan University, Shanghai 200433, China;*
[3] *Physics Department, The Hong Kong University of Science and Technology, Hong Kong 999077, China;*
[4] *The Hong Kong University of Science and Technology Shenzhen Research Institute, Shenzhen 518057, China*

Received June 22, 2022; accepted August 10, 2022; published online November 10, 2022

Charge-spin interconversion in magnetic materials is investigated by using the first-principles calculations. In addition to the conventional spin Hall effect (SHE) that requires mutual orthogonality of the charge current, spin-flow direction, and spin polarization, the recently proposed anomalous SHE (ASHE) is confirmed in Mn_2Au and WTe_2. The interaction of the order parameter with conduction electrons leads to sizeable non-zero spin Berry curvatures that give rise to anomalous spin Hall conductivity (ASHC). Our calculations show that the ASHE is intrinsic and originates from the order-parameter-controlled spin-orbit interaction, which generates an extra anomalous effective field. A useful relationship among the order parameter, the spin Berry curvature, and the ASHC is revealed. Our findings provide a new avenue for generating and detecting arbitrary types of spin currents.

anomalous spin Hall effect, spin Berry curvature, order parameter

PACS number(s): 71.10.-d, 74.25.Ha, 75.30-m, 75.40.Cx

Citation: P. Li, J.-Z. Zhang, Z.-X. Guo, T. Min, and X. Wang, Intrinsic anomalous spin Hall effect, Sci. China-Phys. Mech. Astron. **66**, 227511 (2023), https://doi.org/10.1007/s11433-022-1973-x

1 Introduction

The spin Hall effect (SHE) is related to spin current generation or spin accumulation from an electric current [1-4]. Different from an electric current vector that represents the flow of charges, a spin current, which represents an angular momentum flow, is a tensor of rank two with nine components in Cartesian coordinates. The SHE has received a substantial amount of attention and is widely used to generate spin currents that are an indispensable component of spintronics [1-4]. The inverse SHE is a powerful method for detecting spin currents [5, 6].

In the SHE, a charge current along the $\hat{\beta}$ direction in a material with a strong spin-orbit interaction (SOI) can generate a spin current j_α^γ for which the propagation and spin polarization are along the $\hat{\alpha}$ and $\hat{\gamma}$ directions, respectively. The conventional SHE requires that $\hat{\alpha}$, $\hat{\beta}$, and $\hat{\gamma}$ be mutually orthogonal to each other. Recently, Wang [7] proposed that interactions of conduction electrons with order parameters, such as magnetization for ferromagnets and the Néel order for antiferromagnets, can give rise to an anomalous SHE (ASHE). In linear response theory, the spin current j_i^j due to the charge current $\mathbf{J}$ is

$$j_i^j = \frac{\hbar}{2e}\theta_{ijk}^{\mathrm{SH}} J_k, \tag{1}$$

*Corresponding authors (Zhi-Xin Guo, email: zxguo08@xjtu.edu.cn; Xiangrong Wang, email: phxwan@ust.hk)

where $\theta_{ijk}^{\mathrm{SH}}$ is the spin Hall angle tensor of rank three. $i, j, k = 1, 2, 3$ denote the x, y, and z directions, respectively, and the Einstein summation notation is used. Based on the general tensor requirement of a physical quantity, the following can be obtained [7]:

$$\theta_{ijk}^{\mathrm{SH}} = \theta_0\epsilon_{ijk}+[(\theta_1+\theta_2)\delta_{ij}\delta_{kl\neq i}+\theta_1\delta_{ik}\delta_{jl\neq i}+\theta_2\delta_{il}\delta_{jk\neq i}]M_l, \quad (2)$$

where M_l and ϵ_{ijk} are the l-component of **M** and the Levi-Civita symbols, respectively. θ_0 is the usual spin Hall angle that does not depend on **M**, and θ_1 and θ_2 are the two ASHE coefficients. Thus the conventional SHE is non-zero only when i, j, k take different values. In contrast, the terms involving M_l can be non-zero, which leads to non-zero ASHE spin currents, as indicated in Figure 1(f)-(h). This newly proposed ASHE has been directly verified by experiments of the anomalous spin torques generated in Mn_2Au [8] and is in agreement with the details of the observed magnetization-dependent anomalous inverse SHE (AISHE) in the Pt/Co/Pt heterostructure [9], in TbCo alloys [10], and in Co/Pd multilayers [11]. The ASHE overcomes the limitation of the SHE, and the generated spin current can be controlled by order parameters. In particular, the ASHE allows the spin polarization and spin propagation directions to be collinear when the applied electric current is along the direction of the order parameters. Such a spin current can generate an out-of-plane anti-damping spin-orbit torque (SOT) that is crucial to realizing field-free switching of perpendicular magnetization in high-density SOT devices such as SOT-MRAM [12-17].

Although the ASHE concept has been widely recognized, its microscopic origin has yet to be revealed. Recently, first-principles calculations [18,19] were used to study the anomalous spin torques observed in experiments involving ferromagnets and antiferromagnets. However, the discussions are limited to qualitative symmetry analysis [20], and the intrinsic mechanism of ASHE is still elusive [21]. The anomalous spin torques of specific materials cannot be quantitatively computed without knowing the intrinsic mechanism. Such an investigation is particularly desirable in the field of high-performance SOT devices [14, 16, 21].

Using the local spin density approximation theory with the SOI, we investigate the intrinsic ASHE and obtain the following findings. (1) The ASHE originates from the order-parameter-induced extra spin-dependent electric field, which generates anomalous spin currents via the SOI. (2) The an-

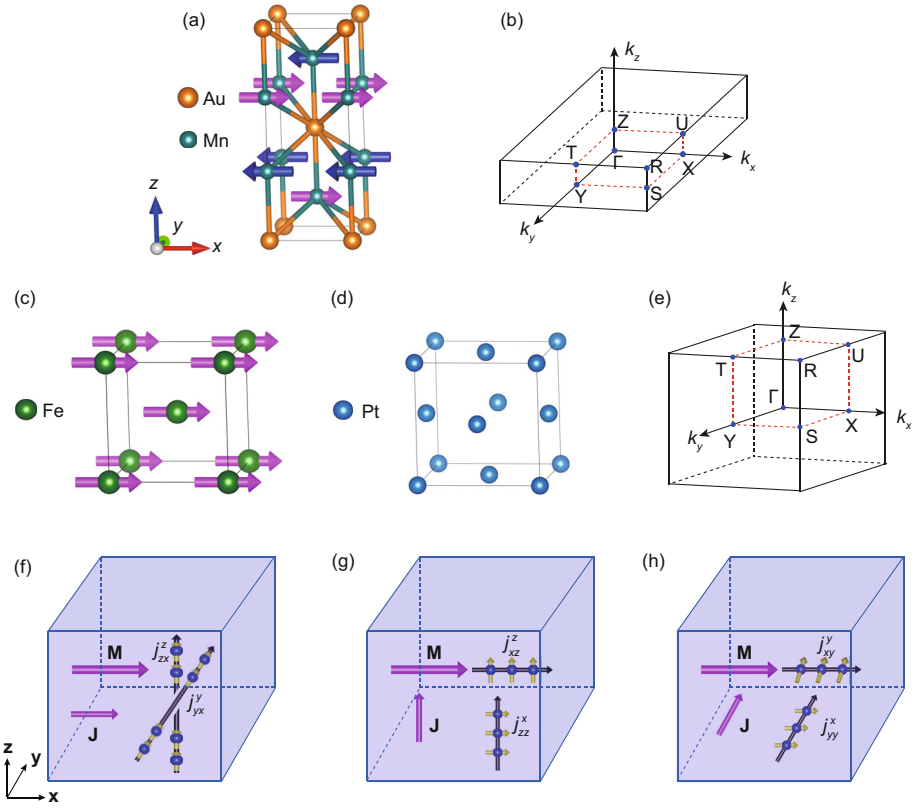

Figure 1 (Color online) The atomic structures, schematic diagrams of the BZ, and schematic diagrams of the ASHE. (a), (c) and (d) show the atomic structures of TET Mn_2Au, BCC Fe, and FCC Pt, respectively. (b), (e) show the corresponding BZs. Note that BCC Fe and FCC Pt have the same BZ structure, shown in (e). (f) illustrates the ASHE with the charge current **J** parallel to the order parameter **M**, and (g), (h) present the ASHE with the charge current **J** perpendicular to **M**.

anomalous spin Hall conductivity (ASHC), which quantitatively represents the strength of the ASHE, can be well described by the spin Berry curvature. (3) There is an intrinsic connection among the order parameter, the spin Berry curvature, and the ASHC.

2 Methods

Our spin-polarized DFT calculations are performed using the Vienna *ab initio* Simulation Package (VASP) [22, 23] and QUANTUM ESPRESSO (QE) [24, 25], in which the projector augmented wave method and a plane wave basis set are applied. We use the VASP for Mn_2Au and WTe_2 and the QE for Fe. All calculations are performed by using spin polarization within the framework of local spin density approximation and generalized gradient approximation for the exchange-correlation energy. The electron exchange-correlation functional is described by the generalized gradient approximation of the Perdew-Burke-Ernzerhof functional [26]. The plane-wave cut-off energy is chosen to be 500 eV for Mn_2Au and WTe_2 and 120 Ry for Fe. Moreover, Γ-centered k meshes of $20\times20\times20$ (Pt), $16\times16\times16$ (Fe), $18\times9\times3$ (WTe_2), and $24\times24\times8$ (Mn_2Au) are adopted in the self-consistent calculations. To better describe the van der Waals (vdW) interaction, the optB86b-vdW functional is adopted in WTe_2 [27, 28]. Then, DFT wave functions are projected onto maximally localized Wannier functions using the WANNIER90 package [29], and the Kubo formula is applied to calculate the SHC [30, 31]. Dense k-point meshes of $150\times150\times150$, $600\times600\times600$, $200\times200\times200$, and $150\times150\times150$ are employed for Pt, Fe, WTe_2, and Mn_2Au, respectively, to perform the BZ integration for the SHC calculations, with a careful convergence test.

3 Results

According to local spin density approximation theory [32, 33], a position-dependent and spin-dependent electric field $\mathbf{E}^p(\mathbf{r})$, which is proportional to the difference of the charge density gradients of the spin-up and spin-down electrons, $[\nabla n^{\uparrow}(\mathbf{r})]$ and $[\nabla n^{\downarrow}(\mathbf{r})]$, can be induced by the magnetic order parameter $\mathbf{M}$ (see Supporting Information). It should be pointed out that the magnetization induced spin-dependent electric field differs from the conventional electric field. The conventional electric field is defined as $\mathbf{E}(\mathbf{r}) = -[\nabla H^{\uparrow}(\mathbf{r}) + \nabla H^{\downarrow}(\mathbf{r})]$, while the spin-dependent electric field is defined as $\mathbf{E}^p(\mathbf{r}) = -[\nabla H^{\uparrow}(\mathbf{r}) - \nabla H^{\downarrow}(\mathbf{r})]$, where $H^{\uparrow}$ and $H^{\downarrow}$ are the Hamiltonians for the spin-up and spin-down electrons, respectively. Hence, the spin-dependent electric field represents the difference in the electric fields between the spin-up and spin-down electrons.

In a collinear magnetic structure with inversion symmetry, the effective spin-dependent electric field (averaged over unit cell), which is defined as $\mathbf{E}^p_{\text{eff}} = \int \mathbf{E}^p(\mathbf{r})\mathrm{d}\mathbf{r} = 0$, is zero. However, $\mathbf{E}^p_{\text{eff}}$ becomes non-zero if the inversion symmetry is broken. Such an $\mathbf{E}^p_{\text{eff}}$ contributes an extra term $H^{\text{eff}}_{\text{SOC}}$ via the SOI (see Supporting Information) to the Hamiltonian,

$$H^{\text{eff}}_{\text{SOC}} = \frac{\hbar e}{2mc^2}\left(\boldsymbol{\sigma}\times\mathbf{E}^p_{\text{eff}}\right)\cdot\mathbf{v}, \tag{3}$$

where $\boldsymbol{\sigma}$ and $\mathbf{v}$ are the Pauli matrices and the electron velocity, respectively. The spin-up and spin-down electrons experience different forces and have different velocities due to a non-zero $H^{\text{eff}}_{\text{SOC}}$. Hence, eq. (3) leads directly to the ASHE as long as $\boldsymbol{\sigma}$ is perpendicular to $\mathbf{E}^p_{\text{eff}}$. For example, in a magnetic material without inversion symmetry in the $\mathbf{z}$ direction, i.e., $E^{p_z}_{\text{eff}} \neq 0$, $H^{\text{eff}}_{\text{SOC}} = \frac{\hbar e}{2mc^2}E^{p_z}_{\text{eff}}\left(\sigma_y v_x - \sigma_x v_y\right)$ is non-zero. Thus, energy splitting between the spin-up and spin-down electrons is generated by the SOI, leading to different velocities. As a result, anomalous spin currents with spin polarization perpendicular to the $\mathbf{z}$, as predicted in Wang's theory [7], are generated (see Supporting Information). It should be noted that the spin-dependent electric field directly correlates to the magnetic order parameter $\mathbf{M}$.

The strength of the ASHE is quantitatively described by the spin Berry curvature. According to the Kubo formula, a spin Hall conductivity $\sigma^{\gamma}_{\alpha\beta}$ of spin-polarization-direction $\hat{\gamma}$ and spin-flow-direction $\hat{\alpha}$ under an external electric field (charge current) along $\hat{\beta}$ can be expressed as [30, 31, 34, 35]:

$$\sigma^{\gamma}_{\alpha\beta} = -\frac{e^2}{\hbar}\frac{1}{VN_k^3}\sum_k\sum_n f_{nk}\Omega^{\gamma}_{n,\alpha\beta}(\mathbf{k}), \tag{4}$$

where V is the cell volume, and N_k^3 is the number of k points in the Brillouin zone (BZ). f_{nk} represents the Fermi-Dirac distribution function, and $\Omega^{\gamma}_{n,\alpha\beta}(\mathbf{k})$ is the band-projected spin Berry curvature, which is defined as:

$$\Omega^{\gamma}_{n,\alpha\beta}(\mathbf{k}) = \hbar^2\sum_{m\neq n}\frac{-2\mathrm{Im}[\langle n\mathbf{k}\,|\,\frac{1}{2}\{\hat{\sigma}_{\gamma},\hat{v}_{\alpha}\}\,|\,m\mathbf{k}\rangle\langle m\mathbf{k}\,|\,\hat{v}_{\beta}\,|\,n\mathbf{k}\rangle]}{(\epsilon_{n\mathbf{k}}-\epsilon_{m\mathbf{k}})^2}. \tag{5}$$

From eqs. (4) and (5), the Hall conductivity $\sigma^{\gamma}_{\alpha\beta}$ is intrinsically determined by the band structure through the spin Berry curvature $\Omega^{\gamma}_{n,\alpha\beta}(\mathbf{k})$ and the density of states. In the conventional SHE, a non-zero $\Omega^{\gamma}_{n,\alpha\beta}(\mathbf{k})$ is expected only when α, β, and γ are mutually orthogonal with each other. However, as discussed below for the case involving the order parameter, a non-zero $\Omega^{\gamma}_{n,\alpha\beta}(\mathbf{k})$ and thus a sizeable ASHE can be obtained when only two of them are mutually perpendicular. In addition, the general Berry curvature formula that requires

$\alpha \neq \beta$ is derived by simply considering the spin direction perpendicular to the velocities of the spin current and charge current ($\alpha \neq \beta \neq \gamma$) [36]. In the case that the spin degree of freedom is not considered, the Berry curvature is a tensor of rank two. For the spin Berry curvature defined in eq. (5), the spin Berry curvature is a tensor of rank three, which is non-zero even for $\alpha = \beta$.

We first consider the tetragonal (TET) Mn_2Au, for which the non-zero ASHE has been experimentally observed [8], as an example. We systematically show an intrinsic connection among the order parameter, the spin Berry curvature and the ASHE. Density functional theory (DFT) calculations are performed to obtain the spin Berry curvature and SHC (see Supporting Information). The crystal structure and schematic BZ diagram of Mn_2Au are illustrated in Figure 1(a) and (b), which verify that Mn_2Au is an antiferromagnetic material with a Néel order parameter **M**. In this study, **M** is fixed in the **x** direction. Hence, as indicated in Figure 1(e)-(g), six non-zero ASHCs are expected, that is, σ^y_{yx} and σ^z_{zx} for the charge current **J** parallel to **M** and σ^x_{zz}, σ^z_{xz}, σ^x_{yy}, and σ^y_{xy} for **J** perpendicular to **M** [7].

The calculated spin Hall conductivities of both the conventional SHC (CSHC) and anomalous SHC (ASHC) components are shown in Table 1. In addition to the large CSHCs, Mn_2Au contains sizeable ASHCs. Moreover, both CSHCs and ASHCs exhibit significant anisotropy, depending on the combination of the spin current, spin polarization, and charge current directions. This characteristic is quite different from that of the conventional SHE, for which the anisotropy is solely from the crystalline structure [20]. For instance, the symmetry of Mn_2Au is expected to give rise to the same CSHCs for σ^z_{xy} and σ^z_{yx}. However, the former [270.58 $(\hbar/e)$S/cm] is more than 3 times larger than the latter [−81.11 $(\hbar/e)$S/cm] because the fourfold rotational symmetry is broken due to **M** along the **x** direction.

Table 1 Spin hall conductivity. The calculated CSHC and ASHC for Fe, Mn_2Au, and Pt. The SHC is denoted as $\sigma^\gamma_{\alpha\beta}$, where α is the direction of the spin current, β is the direction of the applied electrical field, and γ is the direction of the spin polarization of the spin current (unit: $(\hbar/e)$S/cm). The magnetic order parameter **M** is fixed to be along the **x** direction for Fe and Mn_2Au

	SHC	Mn_2Au	Fe	Pt
CSHC	σ^z_{xy}	270.58	120.76	2239.42
	σ^z_{yx}	−81.11	−683.71	−2239.58
ASHC	σ^y_{yx}	15.57	2.87	0.00
	σ^z_{zx}	0.02	−2.89	0.00
	σ^x_{zz}	−10.46	−0.66	0.00
	σ^z_{xz}	−2.95	−3.14	0.00
	σ^x_{yy}	−6.72	0.49	0.00
	σ^y_{xy}	−9.09	1.37	0.00

Moreover, **M** along the **x** direction in Mn_2Au can lead to an additional non-zero spin-dependent electric field in the **z** direction (E^p_z) due to its broken inversion symmetry. According to eq. (3), the non-zero E^p_z induces a spin current with spin polarizations in both the **x** and **y** directions via the SOI and thus leads to sizeable ASHCs. The details are given in the Supporting Information. Our DFT calculations indeed show that the absolute values of the ASHCs with spin polarization in the **x** direction (σ^x_{zz}, σ^x_{yy}) and **y** direction (σ^y_{yx}, σ^y_{xy}) are significantly larger than those with spin polarization in the **z** direction (σ^z_{zx}, σ^z_{xz}) (Table 1). The non-zero values of σ^z_{zx} and σ^z_{xz} may be from other ASHE mechanisms that are beyond the scope of the effective field theory discussed above. Among the six components of the ASHCs, the largest component is σ^y_{yx} [15.57 $(\hbar/e)$S/cm], the magnitude of which reaches 19% of that of its conventional counterpart σ^z_{yx} [−81.11 $(\hbar/e)$S/cm]. Thus a sizeable spin current, the propagation direction of which is collinear to the spin polarization direction, can be effectively generated in Mn_2Au. This result is consistent with experiments [8]. The good agreement between our theoretical derivations and the DFT calculations verifies the intrinsic connection among the order parameter, the spin Berry curvature and the ASHE.

For comparison, we calculate the SHCs of bulk Fe in a body-centered cubic (BCC) structure. As shown in Figure 1(c), although a large **M** is along the **x** direction, $\mathbf{E}^p$ in this system is zero due to the inversion symmetry (see Supporting Information). This means that the order parameter does not directly induce the ASHE in BCC Fe. Our DFT calculations show that despite the considerably large CSHCs, all the ASHCs in Fe are very small, and the ratio of ASHC/CSHC is smaller than 0.5% (Table 1). We also explore the SHCs of non-magnetic Pt in a face-centered cubic (FCC) structure. As shown in Table 1, although the CSHCs of Pt are larger than those of Mn_2Au by an order of magnitude, all the ASHCs are negligible [$<10^{-3}$ $(\hbar/e)$S/cm]. This result confirms the intrinsic connection between the order parameter and the ASHE.

As discussed in Supporting Information, the exchange-correlation potential between the spin-up and spin-down electrons in the Kohn-Sham equations depends on the magnetic order parameter (see Supporting Information). Thus, the spin-polarized DFT calculations under the local spin density approximation can be used to study the effects of the order parameter on the exchange interactions and SOIs [32, 33]. Hence, the calculated electronic structures such as band structures and wave functions contain the effects of the order parameter. Because the spin Berry curvature is directly calculated on the basis of electronic structures (eq. (5)), this result shows an intrinsic connection between the ASHE and the spin Berry curvature. In fact, the intrinsic connection between the spin Berry curvature and the conventional SHE has

been well established in previous studies [36-38].

We further compute the k-resolved spin Berry curvatures for both the CSHCs (Figure 2(a), (c), (e)) and ASHCs (Figure 2(b), (d), (f)) of bulk Mn_2Au, Fe, and Pt. A common feature is that the spin Berry curvatures for the ASHCs are much smaller than those for the CSHCs, in agreement with the experimentally established fact that the ASHCs of these materials are smaller than the CSHCs. In addition, the positive and negative spin Berry curvatures coexist in the BZ, and the CSHC and ASHC values are both determined by the sum of all k points. Thus, although the spin Berry curvature value of Fe is larger than that of Mn_2Au throughout the BZ, its ASHC is much smaller than that of Mn_2Au due to the cancellation of the positive and negative spin Berry curvatures. This result also agrees well with the symmetry analysis above. For Pt, the spin Berry curvatures for the CSHC are dominated by regions with large positive values while the ones for the ASHC are tiny, with an equal weight on positive and negative values, leading to the largest CSHC and a negligible ASHC in comparison with those of Mn_2Au and Fe. The calculated Hall conductivities shown in Table 1 are in good agreement with these spin Berry curvature profiles. The above results clearly show that the spin Berry curvature is intrinsically connected to the conventional SHE and the ASHE.

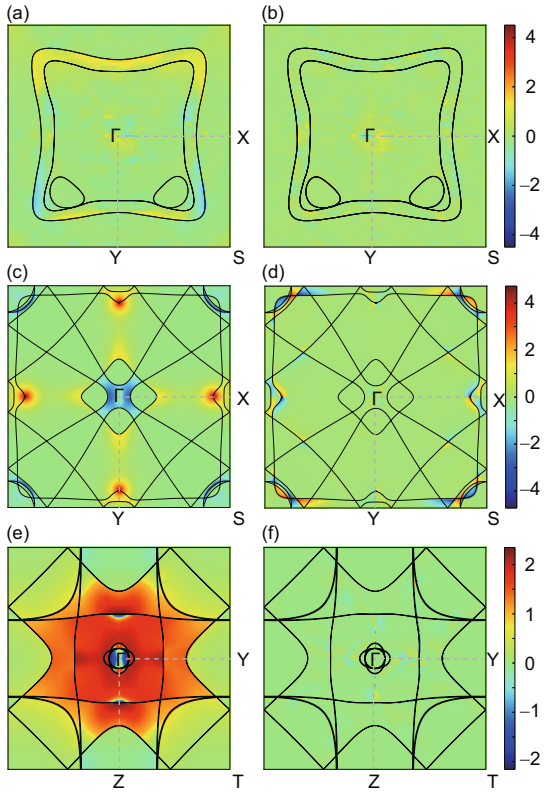

Figure 2 (Color online) Spin Berry curvature in BZ slices. Density plots of spin Berry curvature in BZ slice of $k_z = 0$ for bulk Mn_2Au (a), (b) and Fe (c), (d) and the 2D BZ of $k_x = 0$ for Pt (e), (f). (a), (c), and (e) are the spin Berry curvature σ^z_{yx} of Mn_2Au, σ^z_{xy} of Fe, and σ^z_{xy} of Pt, respectively. (b), (d), and (f) are the spin Berry curvature for ASHC: σ^y_{yx} of Mn_2Au (b), σ^y_{yx} of Fe (d), and σ^y_{yx} of Pt (f), respectively. The black lines denote the intersections of the Fermi surface with the slices. The color code is on a log scale.

4 Discussion and conclusion

The ASHE is not limited to the order parameter in magnetism, and any order parameter breaking the inversion symmetry can lead to a nonzero ASHC via the SOI (such an effect in nonmagnetic materials is denoted as the unconventional SHE). For example, the crystal structure of nonmagnetic materials T_d-WTe_2 (Figure 3(a)) breaks the mirror symmetry with respect to the xz plane and thus leads to a broken inversion symmetry. The broken symmetry in this case induces a non-zero conventional electric field in the **y** direction (E^y_{eff}). According to the SOI Hamiltonian presented in eq. (3), a sizeable unconventional SHE spin current can still be generated when the spin polarization direction is perpendicular to **y** (see Supporting Information). To verify this, we perform DFT calculations on the spin Berry curvature and ASHC of WTe_2, and the results show that σ^z_{zx} = 18.99 $(\hbar/e)$S/cm, reaching 18% of its conventional SHC counterpart σ^y_{zx} [103 $(\hbar/e)$S/cm] [39]. In contrast, we find that σ^z_{zy} has a much smaller value [2.08 $(\hbar/e)$S/cm], which may be attributed to the indirect interaction between E^y_{eff} and v_y. This result is consistent with experimental observations, where the field-free switching of perpendicular magnetization is only observed with the charge current in the **x** direction and not in the **y** direction [14, 40, 41]. In addition, as shown in Figure 3, the positive spin Berry curvature of σ^z_{zx} is much larger than that of σ^z_{zy}. This result confirms the intrinsic connection between the spin Berry curvature and the unconventional SHE in nonmagnetic materials.

In addition, we discuss the novelty of this work in comparison with previous studies [19, 20, 42-44]. The notion of the ASHE was first proposed for spin current generation in ferromagnets from an AHE induced charge current through the conventional SHE, (a phenomenon of SHE+AHE) [19, 42, 43]. The ASHE in our study is the result of the combined effect of the order parameter and the SOI. The physical origins of the two theories are fundamentally different. Moreover, the two theories make distinct predictions: the ASHE in refs. [19, 42, 43] predicts a non-zero spin current only for the noncollinear magnetic order parameter and external electric field. In contrast, the ASHE in this work additionally predicts that the collinear order parameter and electric current generate a spin current with a collinear propagation direction and polarization. The unconventional components of the SHC tensor are also discussed in ref. [20] from a symmetry restriction point of view. Their analysis is valid only when the order

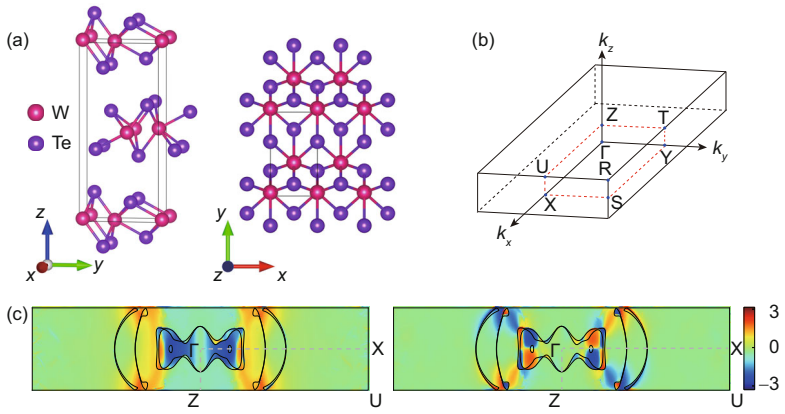

Figure 3 (Color online) The atomic structure, BZ, and spin Berry curvature of WTe_2. The atomic structure (a), schematic diagram of the BZ (b), and k-resolved spin Berry curvature on a log scale in a slice of the 2D BZ at $k_y = 0$ (c) for bulk WTe_2. The left and right panels in (c) show the spin Berry curvature of σ^z_{zx} and σ^z_{zy}, respectively. The black lines show the intersections of the Fermi surface with a slice of the BZ.

parameter does not involve spin-charge conversion, in contrast to the ASHE in this work. In fact, the analysis of ref. [20] fails to yield the ASHC component in Mn_2Au observed in experiment [8]. In addition, the order parameter dependence of the conventional SHE and the AHE in ferromagnets has been recently observed in ferromagnets [44].

Before closing, we emphasize that a dense k-point mesh setting is necessary to guarantee the reliability of the SHC and ASHC calculations. For example, Figure S1 in Supporting Information shows the calculated ASHC σ^y_{xy} of Fe with various k-point mesh settings. Clearly, σ^y_{xy} is as large as 183.48 $(\hbar/e)$S/cm for a small k value of $50\times50\times50$, while its converged value is around 1.0 $(\hbar/e)$S/cm, which can be obtained when the k-point mesh is larger than $400\times400\times400$. Therefore, the k-point mesh convergence test is crucial to the Hall conductivity calculations. This may explain why our results for Fe are different from recent calculations of the same quantities [35].

In summary, we reveal the nature of the intrinsic ASHE: the ASHE originates from the order-parameter-induced spin-dependent electric field, which generates a spin current via the SOI. The intrinsic relationship among the order parameter, the spin Berry curvature and the ASHE is also revealed. The effects of the order parameter on the electronic structure lead to a non-zero spin Berry curvature and thus a sizeable ASHE. The order parameter that gives rise to the ASHE is not limited to the magnetic order parameter. Any order parameter that can break inversion symmetry should contribute to the ASHE. This study is expected to provide an efficient way to search for and optimize materials with large ASHEs, which is particularly important in the design of high-performance SOT spintronic devices.

This work was supported by the National Natural Science Foundation of China (Grant Nos. 12074301, 12004295, and 11974296), and Hong Kong Research Grants Council (Grant Nos. 16300522, 16301619, and 16302321). Ping Li thanks the China's Postdoctoral Science Foundation funded project (Grant No. 2020M673364), and the Open Project of the Key Laboratory of Computational Physical Sciences (Ministry of Education). This research used the resources of the HPCC platform in Xi'an Jiaotong University. We thank Prof. Jian Zhou and Dr. Yongliang Shi for valuable discussions.

Supporting Information

The supporting information is available online at http://phys.scichina.com and https://link.springer.com. The supporting materials are published as submitted, without typesetting or editing. The responsibility for scientific accuracy and content remains entirely with the authors.

1 S. Murakami, N. Nagaosa, and S. C. Zhang, Science **301**, 1348 (2003), arXiv: cond-mat/0308167.
2 J. Sinova, D. Culcer, Q. Niu, N. A. Sinitsyn, T. Jungwirth, and A. H. MacDonald, Phys. Rev. Lett. **92**, 126603 (2004), arXiv: cond-mat/0307663.
3 J. Sinova, S. O. Valenzuela, J. Wunderlich, C. H. Back, and T. Jungwirth, Rev. Mod. Phys. **87**, 1213 (2015), arXiv: 1411.3249.
4 J. E. Hirsch, Phys. Rev. Lett. **83**, 1834 (1999), arXiv: cond-mat/9906160.
5 B. F. Miao, S. Y. Huang, D. Qu, and C. L. Chien, Phys. Rev. Lett. **111**, 066602 (2013).
6 J. C. Rojas-Sánchez, N. Reyren, P. Laczkowski, W. Savero, J. P. Attané, C. Deranlot, M. Jamet, J. M. George, L. Vila, and H. Jaffrés, Phys. Rev. Lett. **112**, 106602 (2014), arXiv: 1312.2717.
7 X. R. Wang, Commun. Phys. **4**, 55 (2021), arXiv: 2008.05303.
8 X. Chen, S. Shi, G. Shi, X. Fan, C. Song, X. Zhou, H. Bai, L. Liao, Y. Zhou, H. Zhang, A. Li, Y. Chen, X. Han, S. Jiang, Z. Zhu, H. Wu, X. Wang, D. Xue, H. Yang, and F. Pan, Nat. Mater. **20**, 800 (2021).

9 T. C. Chuang, D. Qu, S. Y. Huang, and S. F. Lee, Phys. Rev. Res. **2**, 032053 (2020).
10 A. Yagmur, S. Sumi, H. Awano, and K. Tanabe, Phys. Rev. B **103**, 214408 (2021).
11 M. Yang, B. Miao, J. Cheng, K. He, X. Yang, Y. Zeng, Z. Wang, L. Sun, X. Wang, A. Azevedo, S. Bedanta, and H. Ding, Phys. Rev. B **105**, 224426 (2022).
12 M. Cubukcu, O. Boulle, M. Drouard, K. Garello, C. Onur Avci, I. Mihai Miron, J. Langer, B. Ocker, P. Gambardella, and G. Gaudin, Appl. Phys. Lett. **104**, 042406 (2014), arXiv: 1310.8235.
13 L. Liu, C. F. Pai, Y. Li, H. W. Tseng, D. C. Ralph, and R. A. Buhrman, Science **336**, 555 (2016), arXiv: 1203.2875.
14 D. MacNeill, G. M. Stiehl, M. H. D. Guimaraes, R. A. Buhrman, J. Park, and D. C. Ralph, Nat. Phys. **13**, 300 (2017), arXiv: 1605.02712.
15 R. Ramaswamy, J. M. Lee, K. Cai, and H. Yang, Appl. Phys. Rev. **5**, 031107 (2018), arXiv: 1808.06829.
16 L. Liu, C. Zhou, X. Shu, C. Li, T. Zhao, W. Lin, J. Deng, Q. Xie, S. Chen, J. Zhou, R. Guo, H. Wang, J. Yu, S. Shi, P. Yang, S. Pennycook, A. Manchon, and J. Chen, Nat. Nanotechnol. **16**, 277 (2021).
17 Y. Zhang, H. Y. Yuan, X. S. Wang, and X. R. Wang, Phys. Rev. B **97**, 144416 (2018), arXiv: 1802.02415.
18 Y. Zhang, Y. Sun, H. Yang, J. Železný, S. P. P. Parkin, C. Felser, and B. Yan, Phys. Rev. B **95**, 075128 (2017), arXiv: 1610.04034.
19 V. P. Amin, J. Li, M. D. Stiles, and P. M. Haney, Phys. Rev. B **99**, 220405 (2019), arXiv: 1901.04022.
20 M. Seemann, D. Ködderitzsch, S. Wimmer, and H. Ebert, Phys. Rev. B **92**, 155138 (2015), arXiv: 1507.04947.
21 S. Lee, J. Ryu, and B. G. Park, Nat. Nanotechnol. **16**, 227 (2021).
22 G. Kresse, and J. Hafner, Phys. Rev. B **47**, 558 (1993).
23 G. Kresse, and D. Joubert, Phys. Rev. B **59**, 1758 (1999).
24 P. Giannozzi, S. Baroni, N. Bonini, M. Calandra, R. Car, C. Cavazzoni, D. Ceresoli, G. L. Chiarotti, M. Cococcioni, I. Dabo, A. Dal Corso, S. de Gironcoli, S. Fabris, G. Fratesi, R. Gebauer, U. Gerstmann, C. Gougoussis, A. Kokalj, M. Lazzeri, L. Martin-Samos, N. Marzari, F. Mauri, R. Mazzarello, S. Paolini, A. Pasquarello, L. Paulatto, C. Sbraccia, S. Scandolo, G. Sclauzero, A. P. Seitsonen, A. Smogunov, P. Umari, and R. M. Wentzcovitch, J. Phys.-Condens. Matter **21**, 395502 (2009), arXiv: 0906.2569.
25 P. Giannozzi, O. Andreussi, T. Brumme, O. Bunau, M. B. Nardelli, M. Calandra, R. Car, C. Cavazzoni, D. Ceresoli, M. Cococcioni, N. Colonna, I. Carnimeo, A. Dal Corso, S. de Gironcoli, P. Delugas, R. A. DiStasio Jr, A. Ferretti, A. Floris, G. Fratesi, G. Fugallo, R. Gebauer, U. Gerstmann, F. Giustino, T. Gorni, J. Jia, M. Kawamura, H. Y. Ko, A. Kokalj, E. Küçükbenli, M. Lazzeri, M. Marsili, N. Marzari, F. Mauri, N. L. Nguyen, H. V. Nguyen, A. Otero-de-la-Roza, L. Paulatto, S. Poncé, D. Rocca, R. Sabatini, B. Santra, M. Schlipf, A. P. Seitsonen, A. Smogunov, I. Timrov, T. Thonhauser, P. Umari, N. Vast, X. Wu, and S. Baroni, J. Phys.-Condens. Matter **29**, 465901 (2017), arXiv: 1709.10010.
26 J. P. Perdew, K. Burke, and M. Ernzerhof, Phys. Rev. Lett. **77**, 3865 (1996).
27 M. Dion, H. Rydberg, E. Schröder, D. C. Langreth, and B. I. Lundqvist, Phys. Rev. Lett. **92**, 246401 (2004), arXiv: cond-mat/0402105.
28 J. Klimeš, D. R. Bowler, and A. Michaelides, Phys. Rev. B **83**, 195131 (2011), arXiv: 1102.1358.
29 G. Pizzi, V. Vitale, R. Arita, S. Blügel, F. Freimuth, G. Géranton, M. Gibertini, D. Gresch, C. Johnson, T. Koretsune, J. Ibañez-Azpiroz, H. Lee, J. M. Lihm, D. Marchand, A. Marrazzo, Y. Mokrousov, J. I. Mustafa, Y. Nohara, Y. Nomura, L. Paulatto, S. Poncé, T. Ponweiser, J. Qiao, F. Thöle, S. S. Tsirkin, M. Wierzbowska, N. Marzari, D. Vanderbilt, I. Souza, A. A. Mostofi, and J. R. Yates, J. Phys.-Condens. Matter **32**, 165902 (2020), arXiv: 1907.09788.
30 G. Y. Guo, Y. Yao, and Q. Niu, Phys. Rev. Lett. **94**, 226601 (2005), arXiv: cond-mat/0505146.
31 J. Qiao, J. Zhou, Z. Yuan, and W. Zhao, Phys. Rev. B **98**, 214402 (2018), arXiv: 1810.07637.
32 R. Zeller, Comput. Nanosci. **31**, 419 (2006).
33 H. Kronmüller, and S. Parkin, *Handbook of Magnetism and Advanced Magnetic Materials* (Wiley, Chichester, 2007).
34 Q. Lu, P. Li, Z. Guo, G. Dong, B. Peng, X. Zha, T. Min, Z. Zhou, and M. Liu, Nat. Commun. **13**, 1650 (2022).
35 L. Salemi, and P. M. Oppeneer, Phys. Rev. B **106**, 024410 (2022), arXiv: 2203.17025.
36 D. Xiao, M. C. Chang, and Q. Niu, Rev. Mod. Phys. **82**, 1959 (2010), arXiv: 0907.2021.
37 Y. Yao, L. Kleinman, A. H. MacDonald, J. Sinova, T. Jungwirth, D. S. Wang, E. Wang, and Q. Niu, Phys. Rev. Lett. **92**, 037204 (2004), arXiv: cond-mat/0307337.
38 N. Nagaosa, J. Sinova, S. Onoda, A. H. MacDonald, and N. P. Ong, Rev. Mod. Phys. **82**, 1539 (2010), arXiv: 0904.4154.
39 J. Zhou, J. Qiao, A. Bournel, and W. Zhao, Phys. Rev. B **99**, 060408 (2019).
40 B. Zhao, B. Karpiak, D. Khokhriakov, A. Johansson, A. M. Hoque, X. Xu, Y. Jiang, I. Mertig, and S. P. Dash, Adv. Mater. **32**, 2000818 (2020).
41 I. Kao, R. Muzzio, H. Zhang, M. Zhu, J. Gobbo, D. Weber, R. Rao, J. Li, J. H. Edgar, J. E. Goldberger, J. Yan, D. G. Mandrus, J. Hwang, R. Cheng, J. Katoch, and S. Singh, arXiv: 2021.12388.
42 T. Taniguchi, J. Grollier, and M. D. Stiles, Phys. Rev. Appl. **3**, 044001 (2015), arXiv: 1411.4863.
43 K. S. Das, W. Y. Schoemaker, B. J. van Wees, and I. J. Vera-Marun, Phys. Rev. B **96**, 220408 (2017).
44 G. Qu, K. Nakamura, and M. Hayashi, Phys. Rev. B **102**, 144440 (2020), arXiv: 1901.10740.